Stem Cell Reports
Resource
ISSCR
OPEN ACCESS

Robust generation of photoreceptor-dominant retinal organoids from porcine induced pluripotent stem cells

Kimberly L. Edwards,[1,2] Bethany M. Moore,[3] Tyler-Serie Ganser,[2] Praveen Joseph Susaimanickam,[1,2] Kai Sovell,[2] Yolana Martin,[2] Lindsey D. Jager,[2] Ashley M. Willes,[2] Tyra H. Moyer,[2] Lydia Bowar,[2] M. Joseph Phillips,[1,2] Ron Stewart,[3] Li-Fang Chu,[4,5,6,7,*] and David M. Gamm[1,2,8,9,*]

[1]McPherson Eye Research Institute, University of Wisconsin-Madison, Madison, WI, USA
[2]Waisman Center, University of Wisconsin-Madison, Madison, WI, USA
[3]Morgridge Institute for Research, University of Wisconsin-Madison, Madison, WI, USA
[4]Veterinary Medicine, University of Calgary, Calgary, AB, Canada
[5]Reproductive Biology and Regenerative Medicine Research Group, University of Calgary, Calgary, AB, Canada
[6]Alberta Children's Hospital Research Institute, University of Calgary, Calgary, AB, Canada
[7]Biochemistry and Molecular Biology Graduate Program, Cumming School of Medicine, University of Calgary, Calgary, AB, Canada
[8]Department of Ophthalmology and Visual Sciences, University of Wisconsin-Madison, Madison, WI, USA
[9]Lead contact
*Correspondence: lifangjack.chu@ucalgary.ca (L.-F.C.), dgamm@wisc.edu (D.M.G.)
https://doi.org/10.1016/j.stemcr.2025.102425

SUMMARY

Outer retinal degenerative diseases (RDDs) and injuries leading to photoreceptor (PR) loss are prevailing causes of blindness worldwide. While significant progress has been made in the manufacture of human pluripotent stem cell (hPSC)-derived PRs, robust production of pluripotent stem cell (PSC)-PRs from swine, a popular preclinical large animal model, would provide an avenue to collect conspecific functional and safety data to complement human xenograft studies. Toward this goal, we describe the highly efficient generation of PR-dominant porcine induced PSC (piPSC)-derived retinal organoids (ROs) using modifications of our established hPSC-RO differentiation protocol. Porcine iPSC-ROs were characterized using immunocytochemistry (ICC) and single-cell RNA sequencing (scRNA-seq), which revealed the presence and maturation of major neural retina cell types, including PRs and retinal ganglion cells, which possess molecular signatures akin to those found in hPSC-ROs. In late piPSC-ROs, a highly organized outer neuroepithelium was observed with rods and cones possessing outer segments and axon terminals expressing pre-synaptic markers adjacent to dendritic terminals of bipolar cells. The existence of piPSC lines and protocols that support reproducible, scalable production of female and male ROs will facilitate transplant studies in porcine models of retinal injury and RDDs unconfounded by immunological and evolutionary incompatibilities inherent to human xenografts.

INTRODUCTION

Blinding conditions resulting from photoreceptor (PR) degeneration have a high global prevalence (Cross et al., 2022; Wong et al., 2014). Treatments are not available in most cases since mammals, including humans, lack the capacity to regenerate PRs, making it necessary to either replace or bypass them to restore vision. The ability to generate retinal cell types and tissues from human pluripotent stem cells (hPSCs) *in vitro* has facilitated multiple clinical trials focused primarily on reconstructing the retinal pigmented epithelium (RPE), a monolayer of cells that supports the health and function of PRs (Sharma et al., 2019; da Cruz et al., 2018; Kashani et al., 2018; Mandai et al., 2017; Schwartz et al., 2015). In addition, a trial was recently initiated examining the effects of subretinal transplantation of sectioned hPSC-derived retinal organoids (ROs) (Hirami et al., 2023), which contain PRs along with all major cell types found in the neural retina (Capowski et al., 2019; Gasparini et al., 2019; Meyer et al., 2009, 2011).

The preponderance of hPSC-RPE versus hPSC-PR replacement trials is due not only to the relative complexity of clinical PR manufacture but also to challenges demonstrating vision restoration in preclinical animal models using human PR xenografts. In general, all neuronal xenografts are limited by immunological incompatibility and/or evolutionary divergence of synaptic proteins, both of which may hinder functional connectivity between human PRs and non-human host retinal interneurons (Laver and Matsubara, 2017). Notably, recent work has shown that human RO-derived PRs have the intrinsic capacity to (1) respond to light similar to adult primate foveal PRs (Saha et al., 2022), (2) extend neuronal processes (Rempel et al., 2022), and (3) form *de novo* synaptic connections with other hPSC-derived retinal neurons (Ludwig et al., 2023). Therefore, if PRs can be similarly produced from pluripotent stem cells (PSCs) of key animal model species, it stands to reason that they could be used in allograft studies to provide proof of concept for functional cell replacement.

The domestic pig (*Sus scrofa domesticus*) is a favored large animal preclinical model for ocular studies due to its anatomic and physiologic similarity to humans (McCall, 2024; Sanchez et al., 2011; Beauchemin, 1974). In addition,

despite having a significantly shorter gestation period (16 versus 40 weeks), the porcine and human retinae are similarly well developed and organized at birth (McCall, 2024; Wang et al., 2014; Hendrickson and Hicks, 2002; Chandler et al., 1999). These common attributes have led to the creation of numerous swine models of human retinal degenerative diseases (RDDs) or retinal injuries for use in testing the safety and efficacy of experimental treatments, including stem cell-based therapies (Barone et al., 2020, 2023; Choi et al., 2021; Sharma et al., 2019; Ross et al., 2012; Sommer et al., 2011; Kraft et al., 2005).

Given their potential utility in advancing cell replacement strategies for the eye and other organ or tissue systems, extensive efforts have been made since the early 2000s to generate porcine induced pluripotent stem cells (piPSCs) that mirror those derived from humans (Neira et al., 2024; Ezashi et al., 2016). Initial attempts using integrated transgenes failed to demonstrate key characteristics of PSCs, such as survival and self-renewal with extended passage, multi-lineage differentiation potential, and/or teratoma formation (Neira et al., 2024; Ezashi et al., 2016). Even so, rare cells expressing one or more retinal markers, including opsins, could be found in heterogeneous populations differentiated from these early porcine lines (Zhou et al., 2011), fueling continued interest in optimizing piPSC production. Recently, development of porcine PSC-specific culture media (Choi et al., 2019) and transgene-free piPSCs (Conrad et al., 2023) succeeded in overcoming prior shortcomings, allowing reproducible, multi-lineage porcine cell differentiation. However, it remained to be seen whether this new generation of piPSCs could produce ROs.

Toward this end, we devised a method to produce an abundance of piPSC-ROs by adapting an established hPSC-RO differentiation protocol (Capowski et al., 2019) to follow porcine developmental timelines. The piPSC-ROs were characterized by immunocytochemistry (ICC), flow cytometry, and single-cell RNA sequencing (scRNA-seq) and found to contain a high percentage of PRs, with both rods and cones displaying structural features and molecular signatures closely approximating their human RO-derived counterparts. In addition, the molecular identities of porcine RO-derived retinal ganglion cells (RGCs) and other neural retina cell types align with those from hPSC-ROs. This study is the first to demonstrate generation of ROs from piPSCs and to provide an interspecies comparison of the transcriptomes of stem cell-derived retinal cell types. The availability of piPSC-ROs to serve as a conspecific donor cell source for porcine transplant studies addresses multiple confounding issues related to xenotransplantation and complements efforts to develop hPSC-based retinal cell replacement therapies.

RESULTS

piPSCs reproducibly and efficiently generate ROs using a modified human PSC-RO differentiation protocol

To establish a porcine iPSC-RO protocol, female (Figures 1 and S1A) and male (Figure S1B) piPSC lines were differentiated using a human RO differentiation protocol (Capowski et al., 2019) that was adapted to account for the reduced gestational timeline of swine relative to human (Figure 1A). Before initiating differentiation, both piPSC lines were karyotyped and underwent pluripotency confirmation by ICC (Figures S1A and S1B). To maintain piPSC pluripotency, we utilized a feeder layer containing an optimized density of irradiated mouse embryonic fibroblasts (MEFs) (5.4×10^5 MEFs/well of a 6-well plate). Importantly, neither Matrigel nor lower MEF densities (1.9×10^5 MEFs/well) typically employed for human PSC maintenance were successful in keeping piPSCs in a pluripotent state over multiple passages (Figure S1C). For each RO differentiation, embryoid bodies (EBs) were prepared from 4 wells of a 6-well plate containing piPSCs at 80%–90% confluency. Notable temporal differences between swine and human PSC-RO differentiation protocols include (1) addition of bone morphogenetic protein 4 (BMP4) and plating of EBs onto Matrigel-coated plates on day (d) 2 vs. d6, (2) conversion from neural induction medium to retinal differentiation medium at d5 vs. d16, and (3) dissection of adherent RO colonies and transition to free-floating ROs at d11–d13 vs. d25–d35 (Figures 1A and 1B). Quantification of 30 independent, sequential piPSC differentiation runs revealed an average yield of 217 ± 19 ROs per differentiation (minimum = 83; maximum = 401) (Figure 1C). In comparison, direct application of our human PSC retinal differentiation protocol (Capowski et al., 2019) never produced more than four piPSC-ROs per 6-well plate (data not shown). Throughout the differentiation process, piPSC-ROs maintained a phase-bright outer neuroepithelial rim, and, beginning at d80, hair-like protrusions appeared on the surface of piPSC-ROs (Figure 1B) reminiscent of PR outer segments found on human ROs beginning around d150 (Capowski et al., 2019). Thus, using a high-density MEF feeder layer and a shortened differentiation protocol timeline, we were able to reproducibly generate a large number of porcine iPSC-ROs with consistent morphologies.

Early-stage piPSC-ROs are composed of RPCs, RGCs, and early cone PRs

To assess the identity and distribution of retinal cell types in piPSC-ROs at an early stage of differentiation, we first examined expression of selected retinal markers using

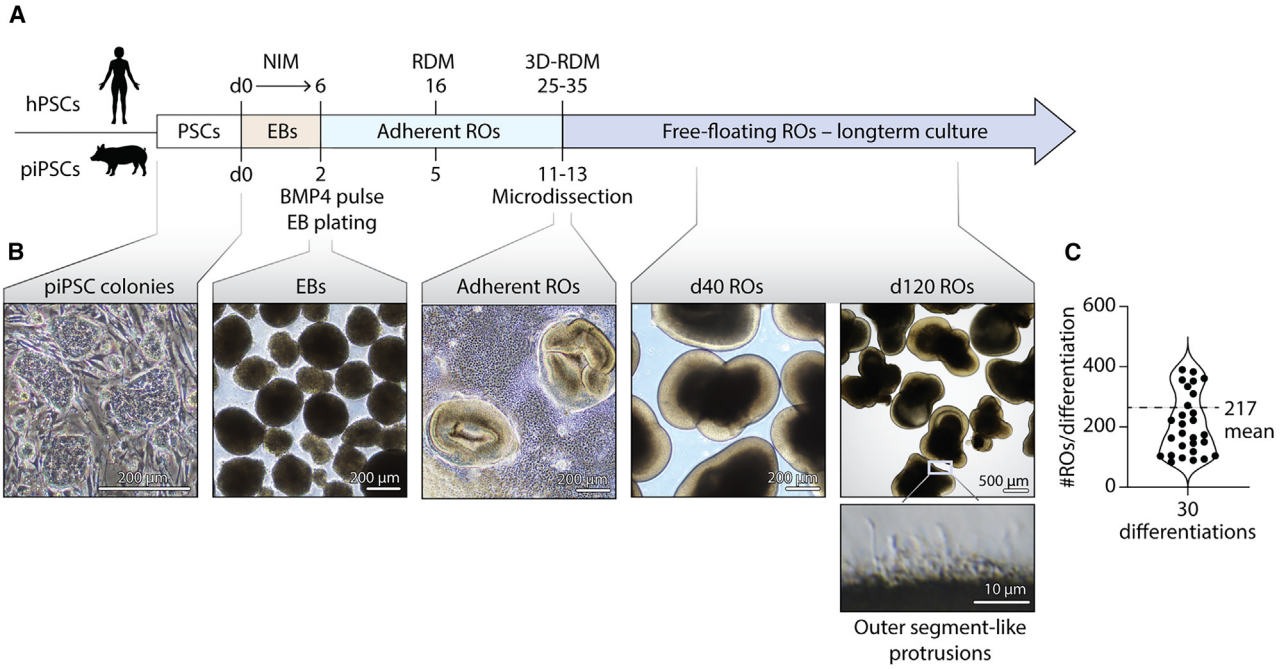

Figure 1. Production and differentiation of ROs from piPSCs

(A) Schematic showing the timing of key steps in the piPSC-RO differentiation protocol used for this study compared to that of an established hPSC-RO differentiation protocol (Capowski et al., 2019).

(B) Representative light microscopic live images of (from left to right) piPSC colonies grown on an optimal density MEF feeder layer, d2 EBs in suspension, d12 adherent RO colonies prior to dissection, and free-floating d40 and d120 ROs in 3D culture after dissection. A higher-magnification image of the surface of a d120 piPSC-RO shows outer segment-like protrusions.

(C) Plot showing the number of piPSC-ROs obtained from each of 30 consecutive differentiations (n = 30 differentiations, mean = 217 ± 19 ROs/differentiation), as indicated by the presence of a compact, uniform, phase-bright outer neuroepithelial rim 2 days after microdissection of adherent cultures. Four wells of a 6-well plate containing 80%–90% confluent piPSCs were used for each differentiation. Scale bars as shown.

ICC. Primary antibodies used for all ICC analyses were validated in the present study using adult porcine retina tissue sections, piPSC-ROs, or piPSCs (Figures S1–S6; Table S1). At d15, VSX2+/Ki67+ proliferating retinal progenitor cells (RPCs) were found across the outer neuroblastic layer of porcine ROs (Figure S3), whereas, by d40, PHH3+ proliferative cells were concentrated at the outer rim (Figures 2A and S4A). OTX2 expression, indicative of newly born PR precursors, was present in cell nuclei throughout the RO neuroepithelium at d40, with more mature, RCVRN-expressing PRs located predominantly along the outer rim (Figures 2A and S4A). The inner portion of d40 piPSC-ROs contained numerous SNCG+ RGCs whose processes aberrantly projected outward toward the RO surface, as has previously been described in human ROs (Figures 2A and S4A) (Capowski et al., 2019).

To further define the cell composition of early piPSC-ROs, scRNA-seq was performed on d35–d41 organoids using the 10× Genomics platform with version 3 chemistry. Five piPSC-ROs from three independent differentiations were pooled to account for potential variability within and between RO cultures, and subsequent analyses were performed as described in Supplemental methods to obtain clusters of similar cells. The clusters were manually annotated using expression of known cell-associated genes, which resulted in the identification of three main cell classes: RPCs, RGCs, and cone PRs (Figure 2B). The full list of genes and parameters employed for cluster identification can be found in Table S2. A fourth cluster of cells was unable to be defined with confidence and therefore was labeled as unknown. Palantir (Setty et al., 2019) pseudotime analysis confirmed that cells within the RGC and cone PR clusters possessed a higher state of differentiation than that within the RPC cluster (Figure 2C). The RPC population expressed high levels of *SFRP2*, *HES5*, and *SOX2* (Figure 2D), whereas the RGC population was characterized by the expression of *GAP43*, *POU4F2* (*BRN3B*), and *SNCG* (Figure 2E). Lastly, the cone PR population was identified via the combined expression of the pan-PR marker *CRX* and the cone genes *PDE6C* and *RXRG* (Figure 2F).

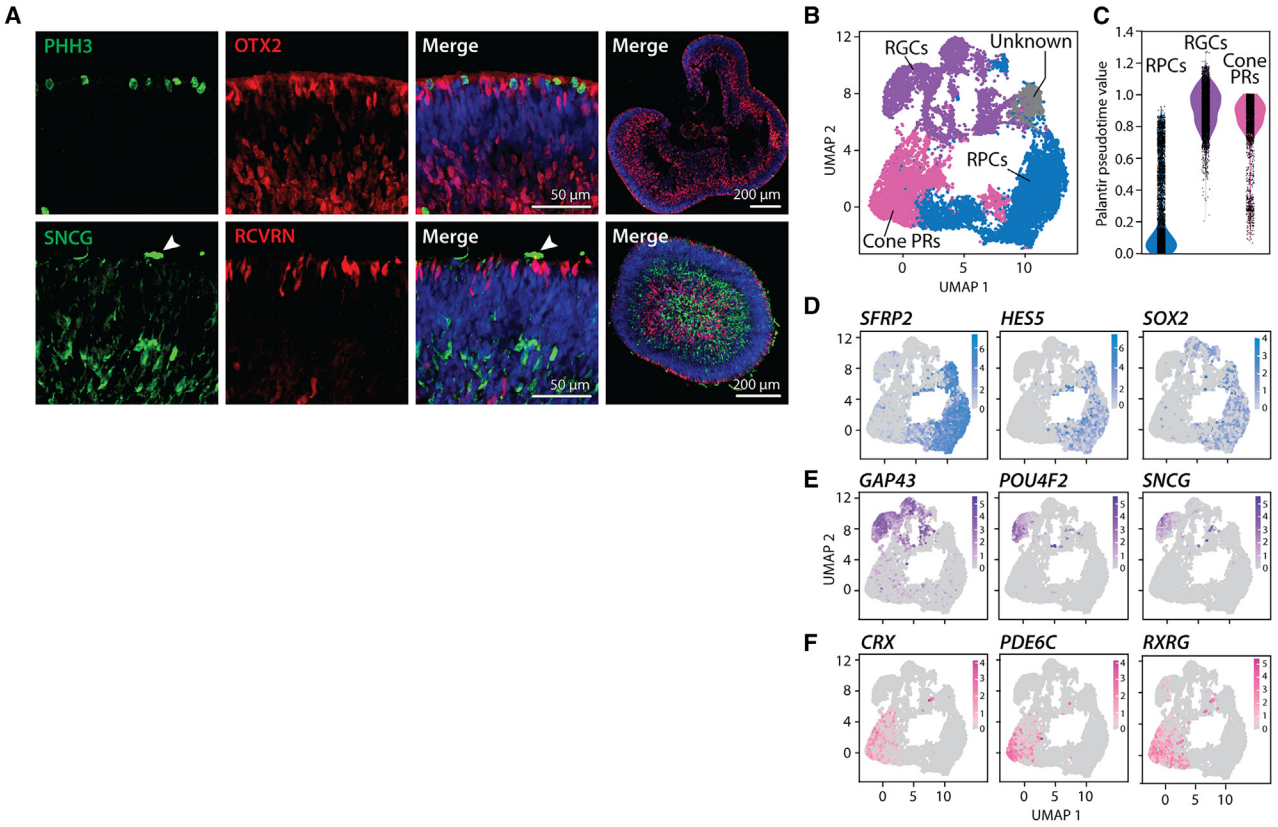

Figure 2. ICC and single-cell RNA-seq analyses of early-stage piPSC-ROs

(A) High- and low-magnification ICC images of d40 female piPSC-ROs showing the presence of PHH3+ proliferating cells along the RO rim with OTX2+ PR precursors found throughout the outer neuroepithelium. Cell bodies of SNCG+ RGCs are located deeper within piPSC-ROs, whose projections (arrowhead) often extend to the RO surface through an outer layer of RCVRN+ PRs.

(B) Uniform manifold approximation and projection (UMAP) of pooled, early-stage (d35-d41) piPSC-ROs was used to visualize the 4 cell cluster annotations (RPC, RGC, cone PR, and unknown).

(C) Palantir values for each identified retinal cell type showed a large separation of RGCs and cones from RPCs in pseudotime.

(D–F) Normalized expression of specific genes expressed in RPCs (D), RGCs (E), and cone PRs (F) projected onto the early-stage piPSC-RO UMAP. Fifteen piPSC-ROs (5 piPSC-ROs from each of 3 independent differentiations) were pooled for early-stage ("d40") scRNA-seq analysis.

Scale bars as shown.

No rod-specific PR genes were present at this stage of RO differentiation (data not shown).

Late-stage piPSC-ROs contain rod and cone PRs, Müller glia, amacrine cells, and bipolar cells

To determine whether piPSC-ROs generate other major neural retinal cell types at later stages of differentiation, ICC was performed on d120 organoids. At this time point, both rod and cone PRs could be identified by the expression of RHO and GNAT2, respectively, within the well-organized outer nuclear layer (ONL) (Figures 3A and S4B). G0α+ rod and cone ON bipolar cells (BPCs) were found in a layer immediately beneath the ONL (Figures 3A and S4B). CRALBP+ Müller glia (MG) cell bodies were also present in the inner nuclear layer (INL) of porcine ROs, with processes extending radially through the ONL (Figure 3A). Of note, at this stage of differentiation, the ONL expressed RCVRN in nearly every PR (compare Figure 3A to Figure 2A) and also expressed RP1, a protein involved in organizing swine cone PR outer segments, near its surface (Figure 3A). PRPH2, an outer segment marker in both rod and cone PRs, was also expressed between d80 and d120 on the surface of piPSC-ROs (Figures S4B and S5A). In contrast, no SNCG+ RGCs remained detectable at d120 by ICC, mirroring the loss of RGCs seen in human ROs over time (Capowski et al., 2019). In addition, we were unable to definitively identify horizontal cells (HCs) and amacrine cells (ACs) in porcine

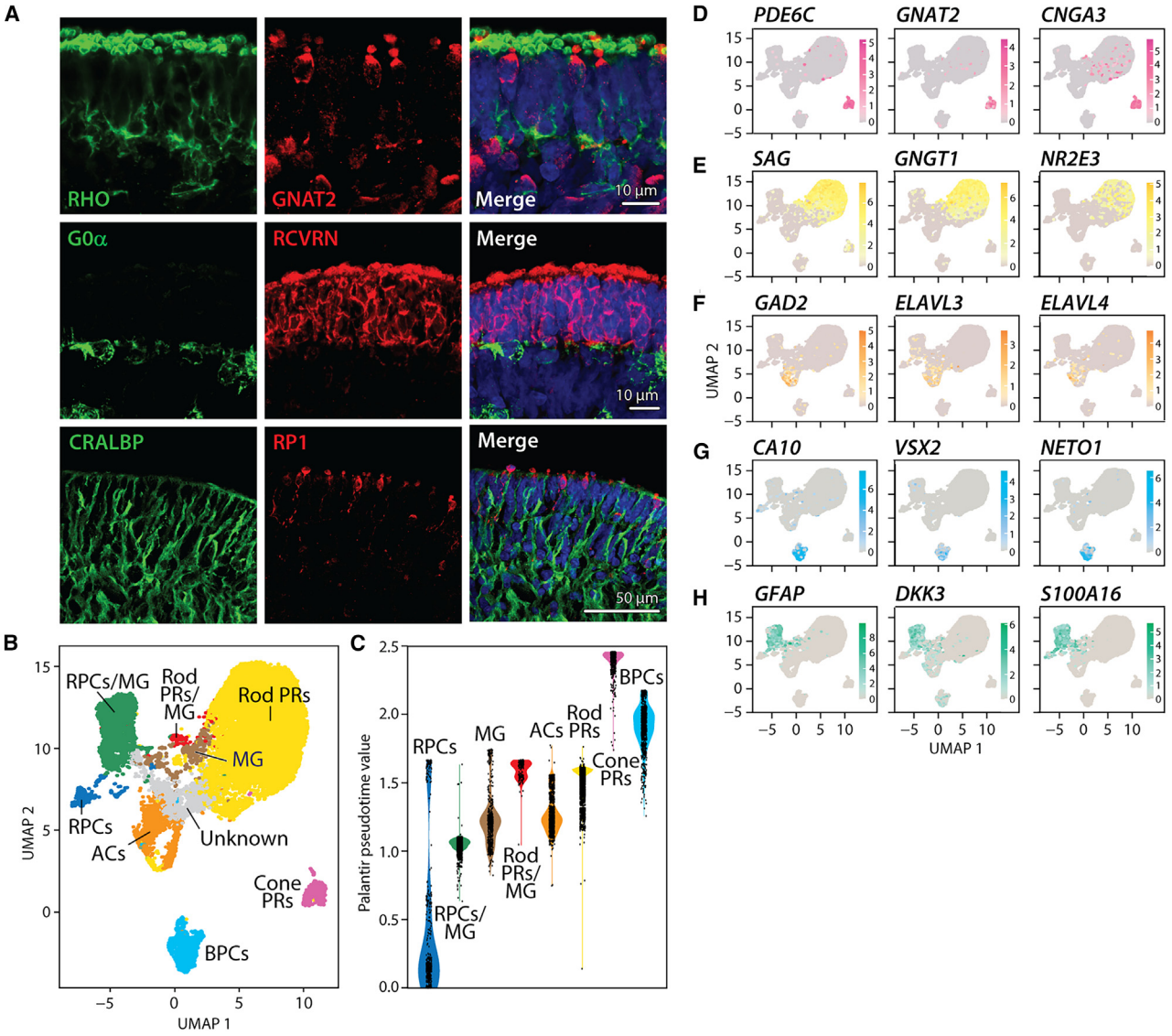

Figure 3. ICC and single-cell RNA-seq analyses of late-stage piPSC-ROs

(A) ICC images of d120 female piPSC-ROs showing RHO staining concentrated at the RO surface with interspersed expression of GNAT2 in cone PRs. G0α is expressed in cone and rod ON BPCs in an inner RO layer beneath the RCVRN+ ONL. CRALBP expression is found in MG cell bodies and radial processes, the latter of which traverse the ONL and form the outer limiting membrane. The ONL is highlighted in the bottom series of images by RP1, a marker of maturing cone PRs in swine.

(B) UMAP plot of late-stage (d118-d122) piPSC-ROs with manual annotations showing 9 cell clusters: cone PRs, rod PRs, BPCs, ACs, MG, RPCs, RPCs/MG, rod PRs/MG, and unknown.

(C) Palantir pseudotime values for each identified cell class in late-stage piPSC-ROs showing the lowest state of differentiation for RPCs and the highest states of differentiation for cone PRs and BPCs.

(D–H) Normalized expression of specific genes expressed in cone PRs (D), rod PRs (E), ACs (F), BPCs (G), and MG (H) projected onto the late-stage piPSC-RO UMAP. Fifteen piPSC-ROs (5 piPSC-ROs from each of 3 independent differentiations) were pooled for late stage ("d120") scRNA-seq analysis.

Scale bars as shown.

iPSC-ROs using available antibodies, in keeping with the weak immunostaining seen in fetal porcine retina (Gudu-ric-Fuchs et al., 2009).

Next, we performed scRNA-seq and analysis on late-stage (d118–d122) piPSC-ROs as described for the early-stage organoids. Clustering identified 8 cell clusters: cone PRs, rod

PRs, BPCs, ACs, MG, RPCs, RPCs/MG, and rod PRs/MG, along with one cluster whose identity was less clear and thus was labeled as unknown (Figure 3B). Palantir pseudotime analysis revealed cone PRs and BPCs to be at the highest state of differentiation among all late-stage retinal cell clusters (Figure 3C). High expression of *PDE6C*, *GNAT2*, and *CNGA3* in the cone cluster (Figure 3D); *SAG*, *GNGT1*, and *NR2E3* in the rod cluster (Figure 3E); *GAD2*, *ELAVL3* (*HUC*), and *ELAVL4* (*HuD*) in the AC cluster (Figure 3F); *CA10*, *VSX2*, and *NETO1* in the BPC cluster (Figure 3G); and *GFAP*, *DKK3*, and *S100A16* in the MG cluster (Figure 3H) was observed. Reverse-transcription PCR analysis confirmed earlier expression of cone- vs. rod-specific genes in piPSC-ROs, broadly verifying the scRNA-seq findings (Figure S5B, primers listed in Table S3). Of note, an HC cluster was not identified via this analysis, and the RPCs/MG and rod PRs/MG clusters expressed multiple markers of two major cell classes and thus were labeled as mixed, or perhaps intermediate, cell populations.

piPSC-ROs generate an abundance of PRs over time

To serve as a useful donor source for future porcine allotransplantation studies, sufficient quantities of desired retinal cell types need to be obtained from piPSC-ROs. Therefore, after broadly identifying the retinal cell classes present in early- and late-stage piPSC-ROs (Figures 2 and 3), we sought to determine their relative abundance over time. Proportional analysis of the early- and late-stage scRNA-seq data revealed that early piPSC-ROs are primarily composed of RPCs (40.0%) with RGCs and cone PRs accounting for the majority of remaining cells (29.0% and 25.5%, respectively) (Figure 4A). In contrast, the major cell population in late piPSC-ROs is rod PRs (60.1%), followed by RPCs/MG (13.0%), ACs (6.4%), BPCs (5.20%), MG (2.90%), cone PRs (2.70%), RPCs (2.20%), and rod PRs/MG (0.80%). The proportion of unidentifiable cells was similar at early and late stages of differentiation (5.50% and 6.70%, respectively). To more rigorously analyze the differential composition and variability in our datasets, we employed sccomp (Mangiola et al., 2023), a recently developed method that models data count distribution, compositionality, group-specific variability, and proportion mean-variability association, while also taking outliers into account. Sccomp confirmed a significant difference in RO cell type composition over time, with RGCs, RPCs, and cone PRs comprising the major populations in early-stage ROs, whereas rod PRs, ACs, RPCs/MG, BPCs, and MG predominate in late-stage ROs. Only the rod PRs/MG population failed to demonstrate significance by sccomp across the two time points, likely because there were so few cells of this type in the later time point that it could not be distinguished from zero (Figure 4B).

Given that PRs hold particular value for retinal allograft studies in preclinical porcine models of outer RDDs, we further examined their production in piPSC-ROs over time using ICC and flow cytometry. RCVRN specifically labels PRs within the adult porcine retina and in piPSC-ROs (Guduric-Fuchs et al., 2009) (Figure S6A) and thus was used as a definitive marker for the overall PR population. At d40, cell bodies of RCVRN+ PRs were detected by ICC in the inner region of the organoids with processes projecting outward toward the surface. Between d80 and d120, an increasingly thick, organized ONL layer composed of PRs developed at the outer rim of ROs, concurrent with a decline in the presence of RCVRN+ PR cell bodies deeper within the organoids (Figure 4C) (Rempel et al., 2022). To quantify the percentage of RCVRN+ PR cells in piPSC-ROs at these time points, flow cytometry on fixed and immunostained cells was performed ($n = 3$ independent differentiations; ≥ 10 piPSC-ROs per differentiation) (Figures S6B and S6C). The percentage of RCVRN+ PRs significantly increased between each time point, from 20.1% ± 1.2% at d40 to 51.6% ± 2.01% at d80 to 73.7% ± 2.1% at d120 ($p < 0.0001$ between d40 and d80; $p = 0.0004$ between d80 and d120) (Figure 4D). These percentages closely approximate those obtained for the PR population from the scRNA-seq compositional analyses.

The cellular organization of mature piPSC-ROs mimics that of adult porcine outer retina

To determine the capacity of piPSC-ROs to adopt a cellular organization akin to native porcine retina, organoids were maintained in culture for up to 190 days, whereupon they were sectioned and immunostained alongside sections of adult porcine retina. Like adult porcine retina, piPSC-RO-derived M/L Opsin+ cone PRs were found in the outermost portion of the ONL, with the remainder of the ONL composed of RHO+ rod PRs (Figures 5A–5C). However, M/L Opsin+ cones were qualitatively less abundant in organoids compared to adult porcine retina, and M/L Opsin and RHO were distributed throughout their respective RO-PRs, as opposed to being exclusively localized to outer segments as observed in adult porcine retina (Figures 5A–5D). Of note, we were unable to reliably detect S Opsin expression above background in piPSC-ROs using available antibodies. Further examination of M/L Opsin and RHO immunostaining in piPSC-ROs revealed that the cone and rod axons extend to an outer plexiform layer (OPL) beneath the ONL that also expresses the PR pre-synaptic marker VGLUT1 (Figures 5A, 5C, and 5D). Immediately below the piPSC-RO OPL is an INL containing G0α+ BPCs (Figures 5A, 5B, and 5D). Higher magnification of whole RO sections also showed that cone PRs possess typical broad, pedicle-like axon terminals that abut G0α+ BPC processes (Figure 5D). Thus, similar to human ROs,

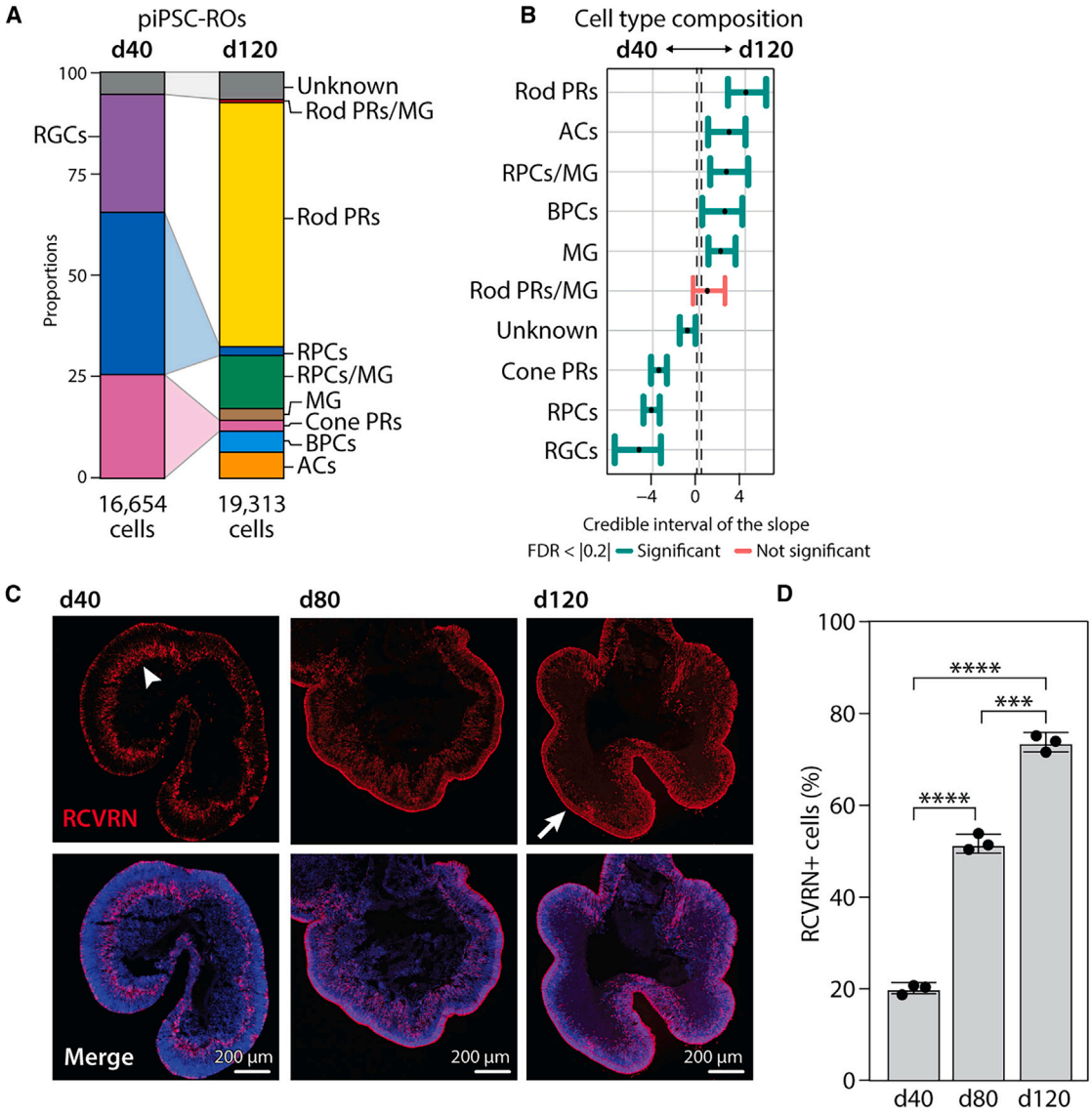

Figure 4. Photoreceptors migrate to form a dense ONL and become the dominant cell population in piPSC-ROs over time

(A) Stacked bar graph showing the proportion of different cell types in female piPSC-ROs at d40 (16,654 total cells) and d120 (19,313 total cells) as determined by scRNA-seq. Cell proportions are listed in the results section.

(B) Analysis of early and late piPSC-RO cell type composition using sccomp. Error bars denote the Bayesian 95% credible interval of the slope between d40 and d120 piPSC-ROs for each cell type, and the central dashed lines represent the minimal effect (0.2) that the hypothesis test is based on. Cell types that comprised a significantly greater proportion of the total cell population in early ROs vs. late ROs or late ROs vs. early ROs are indicated with green error bars to the left or right of the vertical gray line, respectively. The single error bar in pink demarcates a cell type (rod PRs/MG) with no such difference.

(C) Low-magnification, confocal images of whole piPSC-RO sections at d40, d80, and d120 of differentiation showing the location of RCVRN+ PR cells. The arrowhead indicates RCVRN+ PRs primarily localized within a deeper layer at d40, with progressive formation of a dense ONL (arrow) by d120.

(D) Percentage of RCVRN+ PRs in fixed and immunostained cells of piPSC-ROs at d40, d80, and d120 as determined via flow cytometry. ****$p < 0.0001$, ***$p = 0.0004$; ANOVA *post hoc* Tukey's multiple comparisons test. For each time point, $n = 3$ independent differentiations; ≥ 10 piPSC-ROs per differentiation were pooled.

Scale bars as shown.

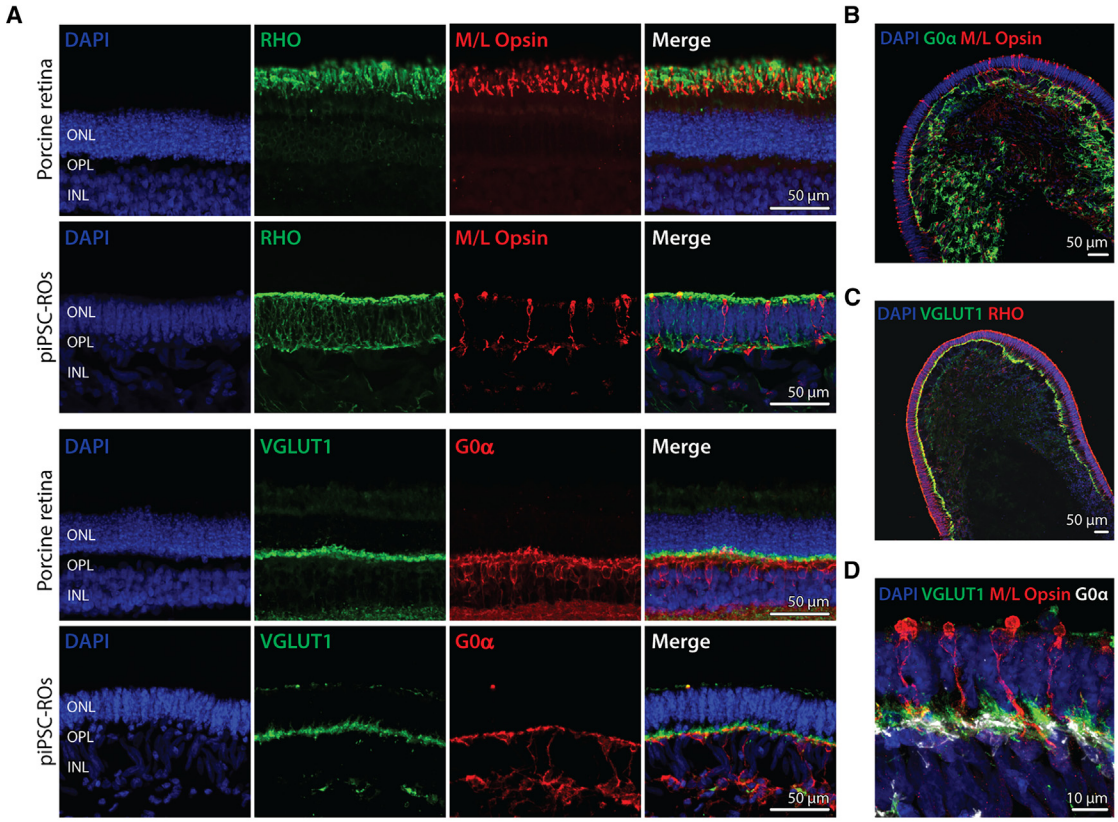

Figure 5. Comparison of outer retinal organization between piPSC-ROs and adult porcine retina

(A) ICC analysis showing layered expression of RHO (rod PRs), M/L Opsin (red and green cone PRs), VGLUT1 (PR pre-synaptic marker), and Gθα (rod and cone ON BPCs) in d190 female piPSC-ROs and adult porcine retina.

(B–D) Low (B and C)- and high (D)-magnification ICC images of d190 piPSC-ROs demonstrating expression of the synaptic marker VGLUT1 at the interface between an ONL containing M/L Opsin+ cone PRs and RHO+ rod PRs and an INL containing Gθα+ rod and cone ON BPCs. Scale bars as shown.

piPSC-ROs are able to self-organize over time to form a layered outer retinal structure that approximates, but does not fully achieve, the full-thickness appearance and precise PR mosaic of native adult porcine retinal tissue.

Developmentally aligned porcine and human ROs possess highly conserved transcriptomes

Our overall goal is to generate a robust source of piPSC-derived retinal cells that can be used as conspecific surrogates for hPSC-derived retinal cells in future preclinical porcine studies. To do so, it is important to assess the cellular and molecular equivalency of porcine ROs and human ROs. We therefore performed an scRNA-seq meta-analysis using our dataset from d120 piPSC-ROs (Figure 3) and an independent dataset from developmentally aligned, d205 human embryonic PSC-ROs (Sridhar et al., 2020) to produce Seurat mapping (Stuart et al., 2019) predictions. The hPSC-RO dataset was first analyzed using the same methods described herein for piPSC-ROs (Figure 6A), whereupon it was employed along with Seurat cell type label transfer to reassign cell identity to the piPSC-RO clusters in an unbiased fashion (Figure 6B). Of note, the d205 hPSC-RO reference dataset does not separate rod and cone PRs and contains some cell types that were not defined in our manually annotated piPSC-RO dataset, such as HCs and immature MG (iMG). Therefore, the re-annotated piPSC-RO dataset also combines rods and cones into a single "PR" cluster and includes HCs and iMG, which were identified based on predictions from the human RO dataset (Figure 6B). In addition to PRs, HCs, and iMG, the cross-species RO meta-analysis identified five other specific retinal cell clusters: ACs, BPCs, RPCs, RPCs/MG, and RGCs.

Overall, porcine iPSC-RO cell identities (particularly PRs and BPCs) were well-predicted by their equivalent human RO cell types based on Seurat mapping prediction scores (on a range of 0–1, with 1 being the highest). PRs and BPCs had a median score of 0.89 and 0.98, respectively,

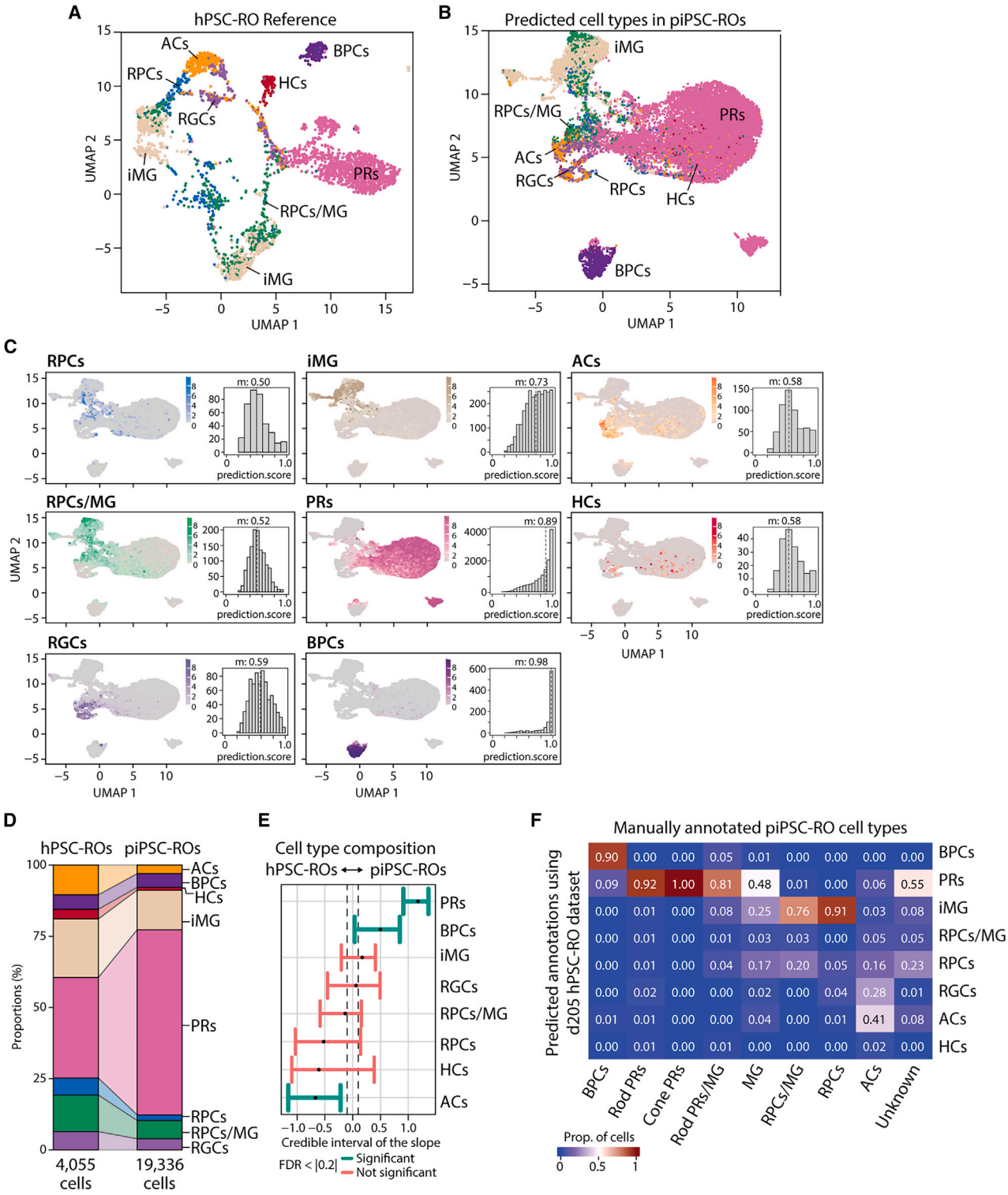

Figure 6. Day 120 piPSC-ROs are transcriptionally comparable to day 205 hPSC-ROs

(A and B) (A) UMAP of a re-analyzed d205 hPSC-RO dataset (Sridhar et al., 2020) used as a reference for (B) Seurat label transfer onto the d120 piPSC-RO UMAP and cell type prediction.

(legend continued on next page)

while other cell types had median scores ranging from 0.50 to 0.73, indicating that PR and BPC cell types are most similar to human (Figure 6C). The proportion of some cell types varied between piPSC-ROs and hPSC-ROs (Figure 6D). Most notably, the percentage of PRs in piPSC-ROs (65%) was almost twice that of hPSC-ROs (35%), while the percentages of ACs and HCs were lower in piPSC-ROs vs. hPSC-ROs (3% vs. 11% [ACs] and <1% vs. 3% [HCs], respectively). Using sccomp analysis, significant differences in cell composition between piPSC-ROs and hPSC-ROs were found for PRs, BPCs, and ACs (Figure 6E). To further investigate the cross-species similarity for each cell type, we assessed how well the manual annotations of piPSC-RO cell types correlated with the predicted cell type annotations derived from the human dataset (Figure 3B vs Figure 6B) (Figure 6F). The vast majority of cone PRs (100%), rod PRs (92%), and BPCs (90%) in the manually annotated dataset were assigned the same identity by the human dataset-predicted annotation, and 91% of RPCs were reassigned as iMG. Other cell types were less closely aligned between the manual and predicted annotations, ranging from 81% (rod PR/MG cluster) to 41% (AC cluster). Interestingly, nearly half of the piPSC-RO cells labeled as ACs by manual annotation were reassigned as RGCs or RPCs by the predicted dataset. Lastly, the unknown cell population in the manually annotated dataset was largely divided between PRs and RPCs in the predicted dataset, which suggests that this population represents an intermediate or immature PR cell type. Overall, these results indicate that multiple retinal cell types present in d120 piPSC-ROs, including PRs, bear a molecular signature similar to those found in d205 hPSC-ROs.

DISCUSSION

An important step in advancing all hPSC-derived retinal cell replacement strategies to the clinic involves preclinical testing in animal models. However, there are limitations to xenograft studies in predicting safety and efficacy in humans owing to immune incompatibilities and structural divergence of key proteins, including those involved in synapse formation and function such as Pikachurin (Laver and Matsubara, 2017). The latter hindrance is particularly relevant for efficacy testing of PR and RGC xenografts, which require functional synaptic connections with host neurons. Furthermore, animals undergoing intense immunosuppression regimens necessary to prevent rejection of xenografts carry a greater risk of systemic toxicity and/or infections, limiting efforts to perform long-term *in vivo* studies. In contrast, allografts can survive using lower levels of immunosuppression that facilitate longitudinal data collection and may better represent protocols to be employed in future human clinical trials.

One approach to addressing the xenograft conundrum is to test human stem cell-derived donor retinal cells in parallel with "'nearest equivalent" donor cells derived from the chosen preclinical animal model species. To do so requires a detailed knowledge of the cellular and molecular signatures of the donor cells across both species. While such knowledge exists for human PSC-ROs (Cowan et al., 2020; Sridhar et al., 2020; Wahle et al., 2023), few methods to generate ROs from PSCs of other species have been described, and most yield exceedingly few organoids (Jacobo Lopez et al., 2022; Völkner et al., 2021; Chen et al., 2016; Eiraku et al., 2011). Failure to maintain pluripotency over multiple passages is a common problem for non-human PSC lines that leads to overall poor lineage-specific differentiation efficiency and reproducibility. If stable pluripotency can be attained, the next hurdle lies in adjusting the timing of retinal differentiation protocols to account for the gestational length of the target species. Lastly, even if consistent and robust manufacture of PSC-ROs can be achieved from a preclinical model source, their retinal progeny may not represent a reasonable facsimile of those derived from hPSC-ROs. Herein, we described the first study in any species to address each of these issues, setting the stage for future efforts to compare retinal cell transplant outcomes between conspecific allografts and human xenografts.

Due to their numerous structural similarities to humans and relative cost-effectiveness compared to non-human primates, swine have grown in popularity as models for developing and testing cell-based therapies. Retinal cell

(C) Prediction score values from Seurat mapping (ranging from 0 to 1, where 1 is the highest score) for each predicted cell type on the d120 piPSC-RO UMAP. Insets show prediction score histograms and medians for each cell type.
(D) Stacked bar graphs showing the proportion of cell types for hPSC-ROs at d205 and piPSC-ROs at d120. Cell proportions are listed in the results section.
(E) Cell type compositional analysis using sccomp. Error bars denote the Bayesian 95% credible interval of the slope between hPSC-ROs and piPSC-ROs cell types, and the central dashed lines represent the minimal effect (0.2) that the hypothesis test is based on. Green error bars indicate cell types that comprise a greater proportion of the total cell population, while pink error bars indicate cell types with no such difference.
(F) Heatmap depicting the relative distribution of cell identities predicted by the human RO dataset (rows) for each manually annotated piPSC-RO cell type (columns), ranging from 0 (blue) to 1 (red).

transplant studies in particular have employed swine as large animal models since they are amenable to the same surgical techniques and outcome assessments used for human subjects (Barone et al., 2023; Sharma et al., 2019). The resulting increased attention from academia, disease foundations, and industry has spurred efforts to generate transgenic swine RDD models, further expanding the utility of the species for therapeutic development (McCall, 2024). Therefore, we focused on producing and characterizing ROs from piPSCs with the goal of providing a consistent, high-volume source of authentic neural retina cells with cellular and molecular properties approximating those of their hPSC-derived counterparts. Building on recent success in generating transgene-free piPSCs (Conrad et al., 2023), we created a robust protocol to generate ROs by (1) optimizing MEF feeder layer density to ensure maintenance of pluripotency and (2) modifying the timing of our existing human protocol (Capowski et al., 2019) to reflect the porcine gestational period that is less than half that of humans. Both steps were key to generating an average of over 200 piPSC-ROs per 6-well plate and are likely important for RO production from PSCs of other species as well. Case in point, a recent publication that sought to produce ROs from rhesus macaque PSCs using an unmodified human retinal differentiation protocol yielded only a few organoids (Jacobo Lopez et al., 2022). Similarly, rote application of our hPSC retinal differentiation protocol to piPSCs generated less than five ROs per 6-well plate.

To examine whether piPSC-ROs have the capacity to mature like human ROs, we employed multiple techniques to identify and quantify cell types within piPSC-ROs over time. By ICC, we identified RGCs, RPCs, and PRs in d40 piPSC-ROs, the latter of which are likely cones, since they are born much earlier than rods in mammals (Swaroop et al., 2010; Wang et al., 2014), and rod markers were not present in d40 porcine ROs. However, due to a lack of antibodies that identify early piPSC-derived cones, we were unable to unequivocally define the subtype of d40 PRs by ICC. Instead, scRNA-seq analysis confirmed both the presence of cone PRs and the absence of rods at this time point. By d120, we identified BPCs, MG, and both RHO+ rods and GNAT2+ cone PRs by ICC. ACs and HCs were unassignable at d120 by ICC, again due to a lack of suitable primary antibodies, but both populations were present by manually annotated and/or predicted scRNA-seq analysis. Seurat mapping predictions showed that numerous retinal cell types generated by piPSC-ROs at d120 were highly analogous to those of d205 hPSC-ROs (particularly cones, rods, and BPCs), suggesting that porcine and human ROs are developmentally equivalent at these time points. A similar cross-species comparison of RGCs could not be performed due to their near absence in later-stage porcine and human ROs. Future scRNA-seq analyses will incorporate earlier time points to better assess interspecies RGC transcriptomic equivalency and attempt to identify RGC subtypes in piPSC-ROs.

While numerous similarities between porcine and human ROs were observed, some differences were also evident. For example, based on scRNA-seq datasets used in our study and others', porcine ROs can yield nearly twice the overall percentage of PRs compared to human ROs, albeit with a higher rod:cone ratio (Sridhar et al., 2020; Cowan et al., 2020). In addition, PRs from porcine ROs had shorter outer segment-like structures than what is typically observed in human ROs. The species-specific underpinnings of these findings are not known but could reflect intrinsic differences in the default programming of RPCs and/or the maturation of PRs derived from piPSCs vs. hPSCs *in vitro*. If so, further modification of porcine RO protocols to manipulate rod:cone ratios and PR development is likely possible.

In summary, we present the first report of RO generation from porcine iPSCs and the first interspecies comparison of stem cell-derived ROs using scRNA-seq. Our findings, combined with those using rhesus macaque and small animal PSCs (Georges et al., 2023; Chen et al., 2016; Osakada et al., 2008), suggest that ROs across multiple species rely on intrinsic programming as they differentiate along their respective developmental timelines. Our study also emphasizes the importance of optimizing early steps in retinal differentiation protocols since, once formed, ROs mature in a predominantly autonomous manner. Given their authenticity and production capacity, piPSC-ROs offer an excellent donor source to test the potential of PRs, RGCs, and other neural retinal cell types to functionally integrate into porcine models of retinal injury and RDDs. Toward this end, we have generated ROs from both female and male piPSC lines to allow definitive identification of donor cells via sex chromosome analysis in gender mismatched recipient swine. Future allograft studies using porcine ROs will help refine retinal cell replacement strategies and enable investigation of ocular immune responses to conspecific subretinal transplants.

METHODS

Retinal differentiation of piPSCs

The piPSC lines obtained from Dr. Li-Fang Chu (Conrad et al., 2023) were differentiated to ROs using a modified hPSC differentiation protocol (Capowski et al., 2019). Details regarding piPSC culture maintenance and RO differentiation are available in supplemental information.

ICC

Cryosections of fixed porcine ROs were immunostained for markers of different neural retinal cell types using primary

antibodies listed in Table S1. Imaging was performed using a Nikon A1R confocal microscope (Nikon, USA). Further details are available in supplemental information.

scRNA-seq and data analysis

Single-cell suspensions from porcine ROs were prepared at specified time points and subjected to scRNA-seq using 10× Genomics Chromium Next GEM reagents according to the manufacturer's guidelines. After quality control analysis, Seurat R package version 4.4.0 (Hao et al., 2021) was used for further data processing. After normalization, variable features were selected using Scry R package version 1.10.0 (https://doi.org/10.18129/B9.bioc.scry). Datasets were subsequently subjected to principal-component analysis, sample clustering, and differential gene expression analyses. See supplemental information for a full description of the methods employed.

For detailed experimental procedures, please see supplemental information.

RESOURCE AVAILABILITY

Lead contact

Requests for further information and resources should be directed to and will be fulfilled by the lead contact, David M. Gamm (E-mail: dgamm@wisc.edu; Phone: 608-261-1516).

Materials availability

This study did not generate new unique reagents.

Data and code availability

The scRNA-seq data are available through NCBI GEO, accession number GSE278658. For code availability, please refer to https://github.com/stewart-lab/scRNAseq_library and https://github.com/stewart-lab/scRNAseq_downstream.

ACKNOWLEDGMENTS

This work was supported by the U.S. Department of Defense (W81XWH2010655) (D.M.G.) and the UW-Madison Department of Ophthalmology and Visual Sciences T32 Award (EY027721) (K.L.E.) and in part by a gift from Arthur and Nancy Nesbitt, the Sandra Lemke Trout Chair in Eye Research, the Retina Research Foundation Emmett A. Humble Distinguished Directorship of the McPherson Eye Research Institute (D.M.G.), and an unrestricted grant from Research to Prevent Blindness to the UW-Madison Department of Ophthalmology and Visual Sciences. We appreciate the use of equipment in the University of Wisconsin Carbone Cancer Center Flow Cytometry Laboratory (Support Grant P30 CA014520). We also acknowledge the UW-Madison Department of Pathology and Laboratory Medicine for the use of its facilities and services, the Waisman Center Cellular and Molecular Neuroscience Core (NICHD U54 HD090255), the UW-Madison Biotechnology Center's Gene Expression Center Core Facility (research resource identifier – RRID:SCR_017757), the DNA sequencing facility (RRID:SCR_017759), and the UW-Madison Biotechnology Center Bioinformatics Resource Center Core Facility (RRID:SCR_017799). The authors thank Dr. Divya Sinha for assistance with the development of the flow cytometry protocol, Jack Freeman for help in the development of the single-cell pipeline, and H. Adam Steinberg (Art for Science) for assistance in figure preparation.

AUTHOR CONTRIBUTIONS

K.L.E., methodology, formal analysis, investigation, writing (original draft), supervision, and formal analysis; B.M.M., methodology, software, validation, formal analysis, data curation, and writing (review and editing); T.-S.G., P.J.S., K.S., Y.M., L.D.J., A.M.W., T.H.M., and L.B., investigation; M.J.P., conceptualization, writing (review and editing), supervision, and funding acquisition; R.S., supervision; L.-F.C., resources and writing (review and editing); D.M.G., conceptualization, resources, writing (original draft and review and editing), visualization, supervision, project administration, and funding acquisition.

DECLARATION OF INTERESTS

The authors declare no competing interests.

SUPPLEMENTAL INFORMATION

Supplemental information can be found online at https://doi.org/10.1016/j.stemcr.2025.102425.

Received: September 26, 2024
Revised: January 31, 2025
Accepted: February 3, 2025
Published: March 6, 2025

REFERENCES

Barone, F., Muscatello, L.V., Ventrella, D., Elmi, A., Romagnoli, N., Mandrioli, L., Maya-Vetencourt, J.F., Bombardi, C., Mete, M., Sarli, G., et al. (2020). The porcine iodoacetic acid model of retinal degeneration: Morpho-functional characterization of the visual system. Exp. Eye Res. *193*, 107979. https://doi.org/10.1016/j.exer.2020.107979.

Barone, F., Amaral, J., Bunea, I., Farnoodian, M., Gupta, R., Gupta, R., Baker, D., Phillips, M.J., Blanch, R.J., Maminishkis, A., et al. (2023). A Versatile Laser-Induced Porcine Model of Outer Retinal and Choroidal Degeneration for Preclinical Testing (American Society for Clinical Investigation).

Beauchemin, M.L. (1974). The fine structure of the pig's retina. Albrecht Von Graefes Arch. Klin. Exp. Ophthalmol. *190*, 27–45. https://doi.org/10.1007/BF00414333.

Capowski, E.E., Samimi, K., Mayerl, S.J., Phillips, M.J., Pinilla, I., Howden, S.E., Saha, J., Jansen, A.D., Edwards, K.L., Jager, L.D., et al. (2019). Reproducibility and staging of 3D human retinal organoids across multiple pluripotent stem cell lines. Dev. Camb. Engl. *146*, dev171686. https://doi.org/10.1242/dev.171686.

Chandler, M.J., Smith, P.J., Samuelson, D.A., and MacKay, E.O. (1999). Photoreceptor density of the domestic pig retina. Vet. Ophthalmol. *2*, 179–184.

Chen, H.Y., Kaya, K.D., Dong, L., and Swaroop, A. (2016). Three-dimensional retinal organoids from mouse pluripotent stem cells mimic *in vivo* development with enhanced stratification and rod photoreceptor differentiation. Mol. Vis. *22*, 1077–1094.

Choi, K.-E., Anh, V.T.Q., Kim, J.T., Yun, C., Cha, S., Ahn, J., Goo, Y.S., and Kim, S.-W. (2021). An experimental pig model with outer retinal degeneration induced by temporary intravitreal loading of N-methyl-N-nitrosourea during vitrectomy. Sci. Rep. *11*, 258. https://doi.org/10.1038/s41598-020-79437-1.

Choi, K.-H., Lee, D.-K., Kim, S.W., Woo, S.-H., Kim, D.-Y., and Lee, C.-K. (2019). Chemically Defined Media Can Maintain Pig Pluripotency Network In Vitro. Stem Cell Rep. *13*, 221–234. https://doi.org/10.1016/j.stemcr.2019.05.028.

Conrad, J.V., Meyer, S., Ramesh, P.S., Neira, J.A., Rusteika, M., Mamott, D., Duffin, B., Bautista, M., Zhang, J., Hiles, E., et al. (2023). Efficient derivation of transgene-free porcine induced pluripotent stem cells enables *in vitro* modeling of species-specific developmental timing. Stem Cell Rep. *18*, 2328–2343. https://doi.org/10.1016/j.stemcr.2023.10.009.

Cowan, C.S., Renner, M., De Gennaro, M., Gross-Scherf, B., Goldblum, D., Hou, Y., Munz, M., Rodrigues, T.M., Krol, J., Szikra, T., et al. (2020). Cell Types of the Human Retina and Its Organoids at Single-Cell Resolution. Cell *182*, 1623–1640.e34. https://doi.org/10.1016/j.cell.2020.08.013.

Cross, N., van Steen, C., Zegaoui, Y., Satherley, A., and Angelillo, L. (2022). Retinitis Pigmentosa: Burden of Disease and Current Unmet Needs. Clin. Ophthalmol. *16*, 1993–2010. https://doi.org/10.2147/OPTH.S365486.

da Cruz, L., Fynes, K., Georgiadis, O., Kerby, J., Luo, Y.H., Ahmado, A., Vernon, A., Daniels, J.T., Nommiste, B., Hasan, S.M., et al. (2018). Phase 1 clinical study of an embryonic stem cell-derived retinal pigment epithelium patch in age-related macular degeneration. Nat. Biotechnol. *36*, 328–337. https://doi.org/10.1038/nbt.4114.

Eiraku, M., Takata, N., Ishibashi, H., Kawada, M., Sakakura, E., Okuda, S., Sekiguchi, K., Adachi, T., and Sasai, Y. (2011). Self-organizing optic-cup morphogenesis in three-dimensional culture. Nature *472*, 51–56. https://doi.org/10.1038/nature09941.

Ezashi, T., Yuan, Y., and Roberts, R.M. (2016). Pluripotent Stem Cells from Domesticated Mammals. Annu. Rev. Anim. Biosci. *4*, 223–253. https://doi.org/10.1146/annurev-animal-021815-111202.

Gasparini, S.J., Llonch, S., Borsch, O., and Ader, M. (2019). Transplantation of photoreceptors into the degenerative retina: Current state and future perspectives. Prog. Retin. Eye Res. *69*, 1–37. https://doi.org/10.1016/j.preteyeres.2018.11.001.

Georges, A., Lavergne, A., Mandai, M., Lepiemme, F., Karim, L., Demeulenaere, L., Aguilar, D., Schyns, M., Nguyen, L., Rakic, J.-M., et al. (2023). Comparing the transcriptome of developing native and iPSC-derived mouse retinae by single cell RNA sequencing. Sci. Rep. *13*, 1223. https://doi.org/10.1038/s41598-023-28429-y.

Guduric-Fuchs, J., Ringland, L.J., Gu, P., Dellett, M., Archer, D.B., and Cogliati, T. (2009). Immunohistochemical study of pig retinal development. Mol. Vis. *15*, 1915–1928.

Hao, Y., Hao, S., Andersen-Nissen, E., Mauck, W.M., Zheng, S., Butler, A., Lee, M.J., Wilk, A.J., Darby, C., Zager, M., et al. (2021). Integrated analysis of multimodal single-cell data. Cell *184*, 3573–3587.e29. https://doi.org/10.1016/j.cell.2021.04.048.

Hendrickson, A., and Hicks, D. (2002). Distribution and density of medium- and short-wavelength selective cones in the domestic pig retina. Exp. Eye Res. *74*, 435–444. https://doi.org/10.1006/exer.2002.1181.

Hirami, Y., Mandai, M., Sugita, S., Maeda, A., Maeda, T., Yamamoto, M., Uyama, H., Yokota, S., Fujihara, M., Igeta, M., et al. (2023). Safety and stable survival of stem-cell-derived retinal organoid for 2 years in patients with retinitis pigmentosa. Cell Stem Cell *30*, 1585–1596.e6. https://doi.org/10.1016/j.stem.2023.11.004.

Jacobo Lopez, A., Kim, S., Qian, X., Rogers, J., Stout, J.T., Thomasy, S.M., La Torre, A., Chen, R., and Moshiri, A. (2022). Retinal organoids derived from rhesus macaque iPSCs undergo accelerated differentiation compared to human stem cells. Cell Prolif. *55*, e13198. https://doi.org/10.1111/cpr.13198.

Kashani, A.H., Lebkowski, J.S., Rahhal, F.M., Avery, R.L., Salehi-Had, H., Dang, W., Lin, C.-M., Mitra, D., Zhu, D., Thomas, B.B., et al. (2018). A bioengineered retinal pigment epithelial monolayer for advanced, dry age-related macular degeneration. Sci. Transl. Med. *10*, eaao4097. https://doi.org/10.1126/scitranslmed.aao4097.

Kraft, T.W., Allen, D., Petters, R.M., Hao, Y., Peng, Y.-W., and Wong, F. (2005). Altered light responses of single rod photoreceptors in transgenic pigs expressing P347L or P347S rhodopsin. Mol. Vis. *11*, 1246–1256.

Laver, C.R.J., and Matsubara, J.A. (2017). Structural divergence of essential triad ribbon synapse proteins among placental mammals - Implications for preclinical trials in photoreceptor transplantation therapy. Exp. Eye Res. *159*, 156–167. https://doi.org/10.1016/j.exer.2017.03.005.

Ludwig, A.L., Mayerl, S.J., Gao, Y., Banghart, M., Bacig, C., Fernandez Zepeda, M.A., Zhao, X., and Gamm, D.M. (2023). Re-formation of synaptic connectivity in dissociated human stem cell-derived retinal organoid cultures. Proc. Natl. Acad. Sci. USA *120*, e2213418120. https://doi.org/10.1073/pnas.2213418120.

Mandai, M., Watanabe, A., Kurimoto, Y., Hirami, Y., Morinaga, C., Daimon, T., Fujihara, M., Akimaru, H., Sakai, N., Shibata, Y., et al. (2017). Autologous Induced Stem-Cell–Derived Retinal Cells for Macular Degeneration. N. Engl. J. Med. *376*, 1038–1046. https://doi.org/10.1056/NEJMoa1608368.

Mangiola, S., Roth-Schulze, A.J., Trussart, M., Zozaya-Valdés, E., Ma, M., Gao, Z., Rubin, A.F., Speed, T.P., Shim, H., and Papenfuss, A.T. (2023). sccomp: Robust differential composition and variability analysis for single-cell data. Proc. Natl. Acad. Sci. USA *120*, e2203828120. https://doi.org/10.1073/pnas.2203828120.

McCall, M.A. (2024). Pig Models in Retinal Research and Retinal Disease. Cold Spring Harb. Perspect. Med. *14*, a041296. https://doi.org/10.1101/cshperspect.a041296.

Meyer, J.S., Shearer, R.L., Capowski, E.E., Wright, L.S., Wallace, K.A., McMillan, E.L., Zhang, S.-C., and Gamm, D.M. (2009). Modeling early retinal development with human embryonic and induced pluripotent stem cells. Proc. Natl. Acad. Sci. USA *106*, 16698–16703. https://doi.org/10.1073/pnas.0905245106.

Meyer, J.S., Howden, S.E., Wallace, K.A., Verhoeven, A.D., Wright, L.S., Capowski, E.E., Pinilla, I., Martin, J.M., Tian, S., Stewart, R.,

et al. (2011). Optic Vesicle-like Structures Derived from Human Pluripotent Stem Cells Facilitate a Customized Approach to Retinal Disease Treatment. Stem Cell. *29*, 1206–1218. https://doi.org/10.1002/stem.674.

Neira, J.A., Conrad, J.V., Rusteika, M., and Chu, L.-F. (2024). The progress of induced pluripotent stem cells derived from pigs: a mini review of recent advances. Front. Cell Dev. Biol. *12*, 1371240. https://doi.org/10.3389/fcell.2024.1371240.

Osakada, F., Ikeda, H., Mandai, M., Wataya, T., Watanabe, K., Yoshimura, N., Akaike, A., Sasai, Y., and Takahashi, M. (2008). Toward the generation of rod and cone photoreceptors from mouse, monkey and human embryonic stem cells. Nat. Biotechnol. *26*, 215–224. https://doi.org/10.1038/nbt1384.

Rempel, S.K., Welch, M.J., Ludwig, A.L., Phillips, M.J., Kancherla, Y., Zack, D.J., Gamm, D.M., and Gómez, T.M. (2022). Human photoreceptors switch from autonomous axon extension to cell-mediated process pulling during synaptic marker redistribution. Cell Rep. *39*, 110827. https://doi.org/10.1016/j.celrep.2022.110827.

Ross, J.W., Fernandez de Castro, J.P., Zhao, J., Samuel, M., Walters, E., Rios, C., Bray-Ward, P., Jones, B.W., Marc, R.E., Wang, W., et al. (2012). Generation of an Inbred Miniature Pig Model of Retinitis Pigmentosa. Investig. Ophthalmol. Vis. Sci. *53*, 501–507. https://doi.org/10.1167/iovs.11-8784.

Saha, A., Capowski, E., Fernandez Zepeda, M.A., Nelson, E.C., Gamm, D.M., and Sinha, R. (2022). Cone photoreceptors in human stem cell-derived retinal organoids demonstrate intrinsic light responses that mimic those of primate fovea. Cell Stem Cell *29*, 460–471.e3. https://doi.org/10.1016/j.stem.2022.01.002.

Sanchez, I., Martin, R., Ussa, F., and Fernandez-Bueno, I. (2011). The parameters of the porcine eyeball. Graefes Arch. Clin. Exp. Ophthalmol. *249*, 475–482. https://doi.org/10.1007/s00417-011-1617-9.

Schwartz, S.D., Regillo, C.D., Lam, B.L., Eliott, D., Rosenfeld, P.J., Gregori, N.Z., Hubschman, J.-P., Davis, J.L., Heilwell, G., Spirn, M., et al. (2015). Human embryonic stem cell-derived retinal pigment epithelium in patients with age-related macular degeneration and Stargardt's macular dystrophy: follow-up of two open-label phase 1/2 studies. Lancet Lond. Engl. *385*, 509–516. https://doi.org/10.1016/S0140-6736(14)61376-3.

Setty, M., Kiseliovas, V., Levine, J., Gayoso, A., Mazutis, L., and Pe'er, D. (2019). Characterization of cell fate probabilities in single-cell data with Palantir. Nat. Biotechnol. *37*, 451–460. https://doi.org/10.1038/s41587-019-0068-4.

Sharma, R., Khristov, V., Rising, A., Jha, B.S., Dejene, R., Hotaling, N., Li, Y., Stoddard, J., Stankewicz, C., Wan, Q., et al. (2019). Clinical-grade stem cell-derived retinal pigment epithelium patch rescues retinal degeneration in rodents and pigs. Sci. Transl. Med. *11*, eaat5580. https://doi.org/10.1126/scitranslmed.aat5580.

Sommer, J.R., Estrada, J.L., Collins, E.B., Bedell, M., Alexander, C.A., Yang, Z., Hughes, G., Mir, B., Gilger, B.C., Grob, S., et al. (2011). Production of ELOVL4 transgenic pigs: a large animal model for Stargardt-like macular degeneration. Br. J. Ophthalmol. *95*, 1749–1754. https://doi.org/10.1136/bjophthalmol-2011-300417.

Sridhar, A., Hoshino, A., Finkbeiner, C.R., Chitsazan, A., Dai, L., Haugan, A.K., Eschenbacher, K.M., Jackson, D.L., Trapnell, C., Bermingham-McDonogh, O., et al. (2020). Single-Cell Transcriptomic Comparison of Human Fetal Retina, hPSC-Derived Retinal Organoids, and Long-Term Retinal Cultures. Cell Rep. *30*, 1644–1659.e4. https://doi.org/10.1016/j.celrep.2020.01.007.

Stuart, T., Butler, A., Hoffman, P., Hafemeister, C., Papalexi, E., Mauck, W.M., Hao, Y., Stoeckius, M., Smibert, P., and Satija, R. (2019). Comprehensive Integration of Single-Cell Data. Cell *177*, 1888–1902.e21. https://doi.org/10.1016/j.cell.2019.05.031.

Swaroop, A., Kim, D., and Forrest, D. (2010). Transcriptional regulation of photoreceptor development and homeostasis in the mammalian retina. Nat. Rev. Neurosci. *11*, 563–576. https://doi.org/10.1038/nrn2880.

Völkner, M., Kurth, T., Schor, J., Ebner, L.J.A., Bardtke, L., Kavak, C., Hackermüller, J., and Karl, M.O. (2021). Mouse Retinal Organoid Growth and Maintenance in Longer-Term Culture. Front. Cell Dev. Biol. *9*, 645704. https://doi.org/10.3389/fcell.2021.645704.

Wahle, P., Brancati, G., Harmel, C., He, Z., Gut, G., Del Castillo, J.S., Xavier da Silveira Dos Santos, A., Yu, Q., Noser, P., Fleck, J.S., et al. (2023). Multimodal spatiotemporal phenotyping of human retinal organoid development. Nat. Biotechnol. *41*, 1765–1775. https://doi.org/10.1038/s41587-023-01747-2.

Wang, W., Zhou, L., Lee, S.J., Liu, Y., Fernandez de Castro, J., Emery, D., Vukmanic, E., Kaplan, H.J., and Dean, D.C. (2014). Swine Cone and Rod Precursors Arise Sequentially and Display Sequential and Transient Integration and Differentiation Potential Following Transplantation. Investig. Ophthalmol. Vis. Sci. *55*, 301–309. https://doi.org/10.1167/iovs.13-12600.

Wong, W.L., Su, X., Li, X., Cheung, C.M.G., Klein, R., Cheng, C.-Y., and Wong, T.Y. (2014). Global prevalence of age-related macular degeneration and disease burden projection for 2020 and 2040: a systematic review and meta-analysis. Lancet Glob. Health *2*, e106–e116. https://doi.org/10.1016/S2214-109X(13)70145-1.

Zhou, L., Wang, W., Liu, Y., Fernandez de Castro, J., Ezashi, T., Telugu, B.P.V.L., Roberts, R.M., Kaplan, H.J., and Dean, D.C. (2011). Differentiation of induced pluripotent stem cells of swine into rod photoreceptors and their integration into the retina. Stem Cell. *29*, 972–980. https://doi.org/10.1002/stem.637.